

Phase stability and the effect of lattice distortions on electronic properties and half-metallic ferromagnetism of Co₂FeAl Heusler alloy: An ab initio study

Aquil Ahmad^{a)}, S. K. Srivastava, and A. K. Das*

Department of Physics, Indian Institute of Technology Kharagpur, India-721302

*E-mail: *amal@phy.iitkgp.ernet.in; ^{a)}aquil@phy.iitkgp.ac.in*

Abstract

Density functional theory calculations within the generalized gradient approximation are employed to study the ground state of Co₂FeAl. Various magnetic configurations are considered to find out its most stable phase. The ferromagnetic ground state of the Co₂FeAl is energetically observed with an optimized lattice constant of 5.70 Å. Thereafter, the system was subjected under uniform and non-uniform strains to see their effects on spin polarization (P) and half-metallicity. The effect of spin orbit coupling is considered in the present study. Half-metallicity (and 100 % P) is only retained under uniform strains started from 0 to +4%, and dropped rapidly from 90% to 16% for the negative strains started from -1% to -6%. We find that the present system is much sensitive under tetragonal distortions as half-metallicity (and 100% P) is preserved only for the cubic case. The main reason for the loss of half-metallicity is due to the shift of the bands with respect to the Fermi level. We also discuss the influence of these results on spintronics devices.

Keywords

First principles calculations, Phase stability, Heusler alloys, Lattice distortions, half-metallicity

1. Introduction

First half-metallic ferromagnet based on Heusler family was proposed by de Groot et al., in 1983 [1]. Since then, this family created a huge interest to the scientific community due to its potential in spintronic devices [2, 3]. Heusler compounds such as Co₂MnX (X= Ge, Si, Sn) [4], Co₂MnZ (Z= main group elements) [5], Co₂MnZ (Z=Si, Ge) [6], Fe₂CoAl [7, 8] and Fe₂YAl (Y = Ni, Mn, Cr) [9] attracted enormous interest of the researchers. The interesting features of these materials are that they exhibit metallic nature for one spin channel and semiconducting nature in other spin channels; hence attribute 100% spin polarization at the Fermi energy (E_F). This feature can be exploited in (1) spin injection devices [10] with large magnetoresistance (MR) (2) perfect

spin filters [11]. Moreover, these materials have shown their potential for magnetocaloric application [12-14]. Initially, researchers investigated many physical properties such as non-local spin ordering [15], magneto-optical properties [16] related to Heusler alloys (HAs). Later their focus was on the origin of the half-metallic energy gap [17-19], and spin orbit (SO) interaction [20]. There are some compounds, which are non-Heusler (see refs. [21, 22]) exhibit half-metallicity. However, Heusler compounds are still required due to their novel properties such as high magnetic moment, Curie temperature (up to 1000 °C), and low coercivity (for ref., see our previous exp. work on Co_2FeAl alloy [23], and references therein). A 100% spin polarization (P) may be achieved under some careful conditions as few results expect a symmetry break in highly ordered surfaces for e.g., NiMnSb/CdS interfaces [24]. Extensive efforts have been devoted to achieving a direct measurement of spin polarization by means of spin-polarized tunneling [25], Andreev reflection technique [26] and spin-polarized photoemission [27]: unfortunately, the reported value was below 100%. In contrast, half-metallicity was supported by some experiments viz. infrared reflectance spectroscopy [28], and spin-resolved positron annihilation experiment [29]. The high value of magnetoresistance (MR) was not observed in spin-valve using Heusler layers [30]. However, it was observed in powder compact form [31], suggesting that the high value of spin polarization in thin films is difficult to achieve. Electronic structure calculations suggest that structural defects [32] and atomic site disorder [33] reduces the half-metallic (HM) character of Heusler alloys. The effect of structural distortions on the electronic and magnetic properties of some Heusler alloys has been studied in detail [34-36]. Though, the effect of structural deviation (or distortion) from an ideal structure (i.e., cubic) upon half-metallicity and spin polarization (P) is not understood sufficiently, specifically in Co_2FeAl (CFA).

In this paper, first time, we do a systematic studies of ground state properties of CFA alloy by means of phase stability under various magnetic states viz. paramagnetic (PM)/or non-magnetic (NM), ferromagnetic (FM), ferrimagnetic (FiM) and antiferromagnetic (AFM), to find out the most stable ground state. Thereafter, our system was exposed under uniform and non-uniform strains by means of lattice constant related to zero (or unstrained) pressure, to see its effects on P and half-metallicity. The present research is highly instructive in synthesizing thin films, nanostructures/and or heterostructures based on Co_2FeAl . Due to the fact that only, a few percent deviations from the bulk lattice constant results in a loss of 100% P. This study further proves that non-uniform strain is not the only reason for the low-performance of Heusler alloys in spin-based devices.

2. Computational details:

Band structure calculations have been performed using Wien2k computational code [37] based on density functional theory. The accuracy of the electronic structure calculation results strongly depend upon the choices of exchange-correlation functional. Previous studies suggest that general gradient approximation (GGA) is more appropriate for the strongly correlated d-f electron systems such as half-metals [38-40]. Therefore, we use generalized gradient approximation (GGA) [41] of Perdew-Burke-Ernzerhof (PBE). The electronic configurations used for the valence states of Co, Fe, and Al are: $3p^6, 4s^2, 3d^7$; $3p^6, 4s^2, 3d^6$, and $3s^2, 3p^1$ respectively. The non-spherical contribution of the charge density was being considered up to $l_{\max} = 10$ within the muffin-tin (MT) sphere. The muffin-tin sphere radii were chosen as 2.28 a.u. for Co/Fe, and 2.15 a.u. for Al atoms resulting in nearly touching spheres. The cut-off parameter $R_{\text{MT}} \times K_{\max} = 7$ was set for all calculations. The charge density and potential may expand in the interstitial region up to $G_{\max}=12$ (a.u.⁻¹). The grid of $15 \times 15 \times 15$ mesh was used during all calculations. The spin orbit coupling (SOC) effect is considered in this work. The total energy versus volume curve was fitted with the Birch-Murnaghan equation of state [42] to give the optimized parameters.

3. Results and discussion

3.1. Phase stability

Through theoretical investigations are performed to study the physical properties of CFA. Our primary objective was to find the most stable ground state and study its limitation in relation to half-metallicity, spin polarization, Slater-Pauling (SP) rule and magnetic properties when the system undergoes some structural distortions (i.e., deviation from its ideal structure of Cu_2MnAl prototype). Half-metallic ferromagnets (HMFs) which often exhibit 100 % spin polarization at the Fermi energy (E_F), are crucial for their applicability and performance of spintronic devices. It is known that CFA alloy can be crystallized in regular $L2_1$ (Cu_2MnAl prototype) structure (see figure 1(a)) under $Fm\bar{3}m$ space group (# 225) where all atoms belong to four available Wyckoff sites: 4a (0, 0, 0), 4c (0.25, 0.25, 0.25), 4b (0.5, 0.5, 0.5) and 4d (0.75, 0.75, 0.75). Further, it is also known that in FCC lattice, antiferromagnetic ordering (AFM) is difficult to achieve due to the presence

of geometrical frustration in the system so a structural distortion is essential. Tetragonal distortion usually occurs in Heusler alloys [43]. Therefore, to obtain an AFM structure, we construct a supercell of CFA, which takes the space group Pmmm (# 47), as shown in figure 1. Here, the ferromagnetic (FM) planes of Co spins are alternatively arranged in a specific direction [001].

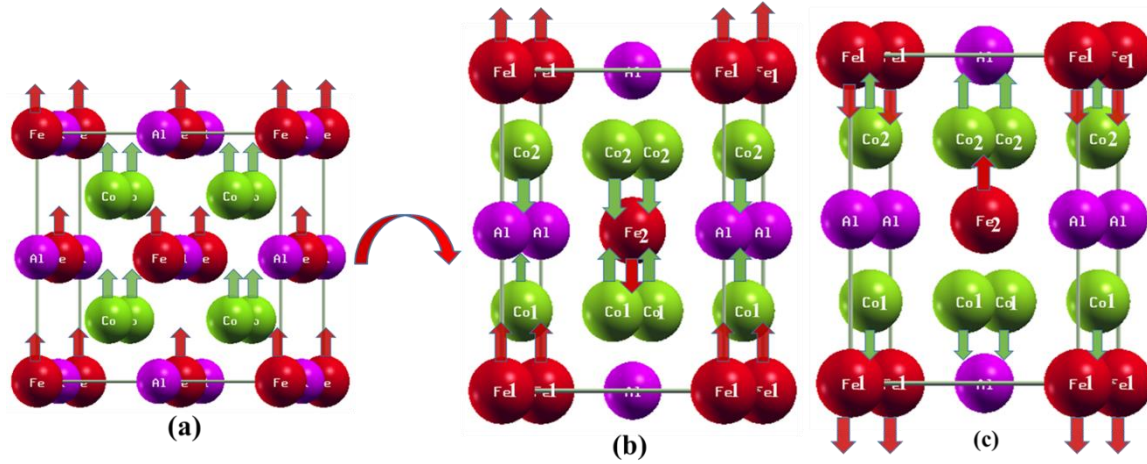


Fig. 1. (Color online) Crystal structure of Co_2FeAl alloy in (a) FM (b) AFM-I (c) AFM-II configurations. All crystal structures have been generated using XCrysDen software [44].

Similarly, FM-planes of Fe spins have also been arranged (see Fig. 1(b, c)) [45].

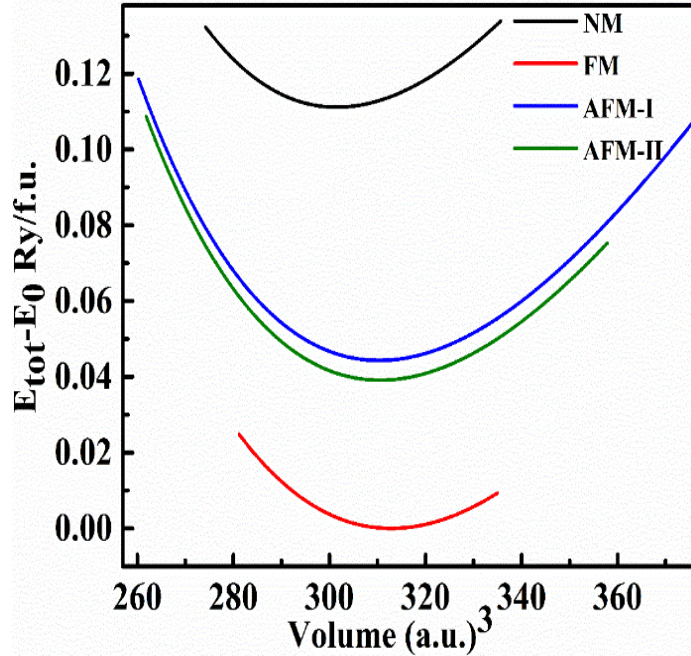


Figure 2. (Color online) Total energy difference ($E_{\text{tot}}-E_0$) as a function of the unit cell volume of Co_2FeAl alloy under NM/or PM, and magnetic (ferromagnetic and antiferromagnetic) configurations. The optimized curve is obtained after fitting with the Birch-Murnaghan equation of state.

At first, to obtain the ground state of CFA, lattice optimizations have been performed in different magnetic states viz. paramagnetic (PM), ferromagnetic (FM), ferrimagnetic (FiM) and antiferromagnetic (AFM). The total energy difference versus volume [$(E_{\text{tot}}-E_0)-V$] curves are presented in figure 2. Note that the ferrimagnetic state was not achieved even after more than 100 iterations in the self-consistent field (scf) cycles.

Parameter	NM (Cubic)	FM (Cubic)	AFM-I (Tetragonal)	AFM-II (Tetragonal)
lattice constants (\AA)	5.72 (previous exp.)* [23], 5.73 (theory)** [46],			
Eq. lattice constants (\AA)	5.63	5.70, 5.69[43]	a = b = 4.02 c = 5.69	a = b = 4.02 c = 5.69
Bulk modulus B (GPa)	211.69	190.64 (this work) (a) 190.19 [calcul.] (b) 239.0 [calcul.] (c) 204.0 [exp.]	193.35	193.50
Derivative of Bulk modulus (B')	4.45	4.60 (a) 4.55	4.74	4.73
Total energy (E_0)	-8605.1407	-8605.2518	-8605.2075	-8605.2127

* At room temperature (RT); (a) Ref. [38, 47]; (b) Ref. [48]; (c) Ref. [49]

** At T=0 K

Table 1. The calculated optimized lattice parameter a_0 (Å), bulk modulus B (GPa) and its pressure derivative B' , equilibrium volume V_0 , and total energy (E_0) per cell of the Co_2FeAl . The other results are presented in the parenthesis.

The Birch-Murnaghan fitted parameters such as optimized lattice constant (a_0), bulk modulus B_0 including its pressure derivate B , and the total energies per cell (E_{tot}) are enlisted in table 1 along with those of the other results shown in brackets for comparison. From figure 2, we established the stability of the ferromagnetic state where we have imposed our CFA system to be either ferrimagnetic, antiferromagnetic, or paramagnetic. On a comparison of the total energy, it is clear that Co_2FeAl alloy energetically prefers FM ordering as its ground state, and hence likely to be observed in experiments. The optimized lattice constant ($a_{\text{opt.}}$) of FM type CFA was found to be 5.70 Å, which closely matches with the experimental one (see table1). This observation is consistent with the experimental results where FM ground state of CFA has earlier been reported [23, 50]. To our knowledge, there are no experimental reports on AFM or FiM ground state of CFA. Figure 3 shows the spin-polarized total and atomically resolved density of states. It is clear that the density of states near the Fermi level (E_F), are dominated by 3d states of Co and Fe atoms. Whenever the majority states are nearly fully occupied, the two peaks in minority states, just above the Fermi level are due to Co and Fe 3d contribution. The broad structure in the lowest energy region between -8.0 and -5.8 eV (not shown) is due to Al (non-magnetic) 3s and 3p states, which are very well separated from 3d states of Co/Fe found between -5.3 to 4 eV. The Fermi-level is

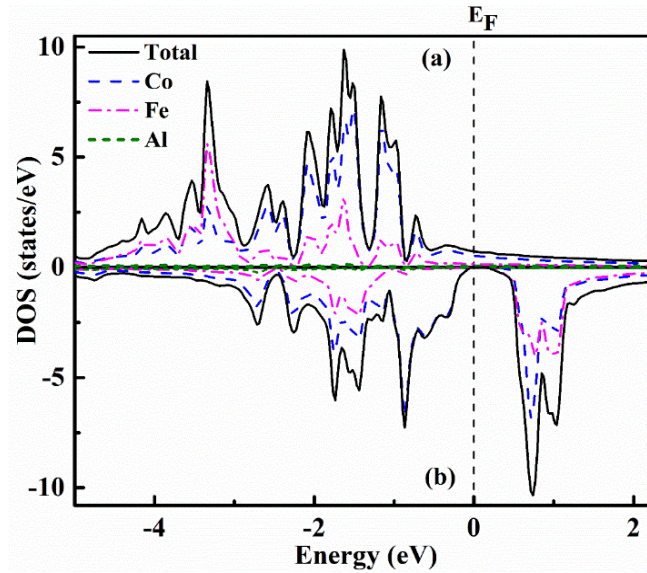


Figure 3. The total and partial DOS of Co₂FeAl alloy are shown of (a) majority (up) and (b) minority (down) spins. The Fermi level (E_F) is set at zero energy.

falling in the gap for minority states, attributing 100% spin polarization at the E_F . It is well described in ref. [17] that for such half-metallic compounds the total magnetic moment should be an integer.

Structure	M_{Co} (μ_B)	M_{Fe} (μ_B)	M_{Al} (μ_B)	M_{Tot}^{Cal} (μ_B)	M_{Tot}^{Rep} (μ_B)	M_{Tot}^{Exp} (μ_B)	M_{Sp} (μ_B)
FM	1.23	2.81	-0.05	5.00	5.08 [43] 4.99 [51]	5.2 (bulk) [52] 5.3-6.5 [23] (Our exp.)	5.0 [17]
AFM-I	Co1/Co2 -0.13/+0.13	Fe1/Fe -2.91/+2.91	Al1/Al2 -0.01/+0.01	0.0			
AFM-II	Co1/Co2 -0.12/+0.12	Fe1/Fe2 +2.91/-2.91	+0.01/-0.01	0.0			

Table 2. The calculated total and partial magnetic moments in FM, AFM-I, and AFM-II state: (M_t), M_{Co} , M_{Fe} , and M_{Al} in μ_B are listed. The other theoretical and experimental results for comparison are shown in brackets.

From the self-consistent field (scf) calculation results (see Table. 2), the total magnetic moment per cell of FM ordered CFA alloy is found to be 5.0 μ_B which is consistent with the Slater-Pauling (SP) rule [17] and hence, resulting a perfect half-metal. It is clear that only Co and Fe atoms are contributed in the total magnetic moment, and Al has a negligible moment. Thus the FM interaction between Co-Fe are the strongest bonding interaction, determining an energy gap of 0.11 eV in the minority-spin band. Due to the covalent hybridization between Co and Fe, bonding and antibonding states are formed which determine the position of the E_F [31].

The Fe atom has largest magnetic moment and couple ferromagnetically to the Co atom. Spin down states essentially represent the characteristic of Co and Fe atoms therefore it is realistic to consider the hybridization between them. The four sp bands are situated far below the E_F hence, inappropriate for the gap. Consequently, the hybridization of the 15 d states of the two Co atoms and one Fe atom are being considered. The hybridization between d-orbitals of the two Co and one Fe atoms is schematically shown in figure 4, to explain the reason for the band gap in Co_2FeAl . First, we sketch the hybridization between the Co atoms as shown in figure 4 (left side). The five d-orbitals of Co comprise of the 3-fold degenerate d_{xy} , d_{yz} , and d_{xz} , and the 2-fold degenerate d_{z^2} , and $d_{x^2-y^2}$ states. The t_{2g} (e_g) orbitals of Co atoms can only pair with the t_{2g} (e_g) orbitals of the other Co atom. The t_{2g} and e_g are bonding orbitals, while t_{1u} and e_u are antibonding orbitals. The degeneracy of the orbitals is represented by the numbers providing the respective orbitals. Now the hybridization scheme is presented between the Co-Co hybridized orbitals and the Fe d-orbitals as shown in right side of figure 4. The doubly degenerate e_g orbitals hybridize with the d_4 (or d_{z^2}) and d_5 ($d_{x^2-y^2}$) orbitals of Fe and form doubly degenerate bonding and antibonding e_g orbitals.

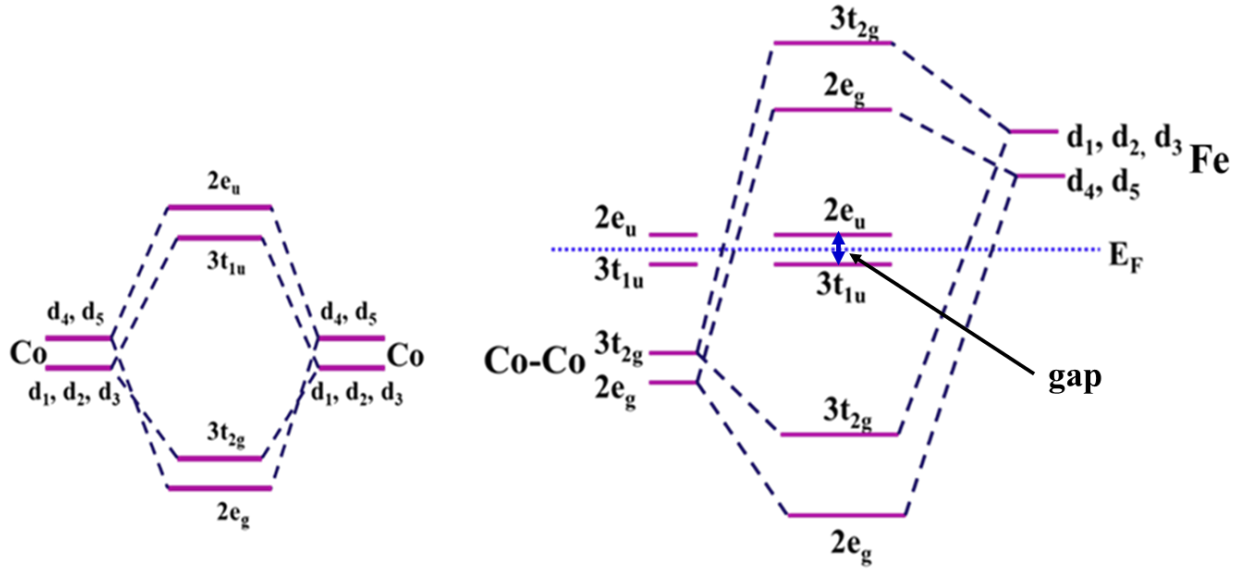


Figure 4. A schematic diagram of possible hybridizations between d orbitals located at different sites in the case of Co_2FeAl compound. For simplicity, d_{xy} , d_{yz} and d_{xz} orbitals are represented by d_1 , d_2 and d_3 , and d_{z^2} and $d_{x^2-y^2}$ orbitals are represented by d_4 and d_5 , respectively. The degeneracy of the corresponding orbital is represented by the coefficients. The t_{2g} and e_g states represent the bonding, and t_{1u} , e_u represent the antibonding orbitals.

The triply degenerated t_{2g} orbitals couple with the d_1 , d_2 , and d_3 orbitals of Fe and form six new hybrid orbitals, three of which are bonding and the other 3 are antibonding. Lastly, the doubly and triply degenerate e_u and t_{1u} orbitals can't couple with any d-state of Fe as these states are orthogonal to e_u and t_{1u} states of Co. The t_{1u} states lie below the Fermi energy whereas e_u states lie above E_F . Therefore, out of 15, eight states are filled and the rest are empty. The E_F falls between the 5 non-bonding Co states in such a way that the 3 t_{1u} bands are fully occupied and the rest 2-bands of e_u are empty. The interaction between Co-Co atoms actually determine the real gap in Co_2FeAl , forming due to the presence of the splitting of e_u and t_{1u} states near the E_F [53].

3.2. Effect of lattice distortions on the electronic and magnetic properties

In this section, we study the effect of lattice distortions on half-metallic ferromagnetism of Co_2FeAl alloy. Initially, the calculation was started from zero strain i.e., at equilibrium lattice constant, $a_{(\text{optim.})} = 5.70 \text{ \AA}$.

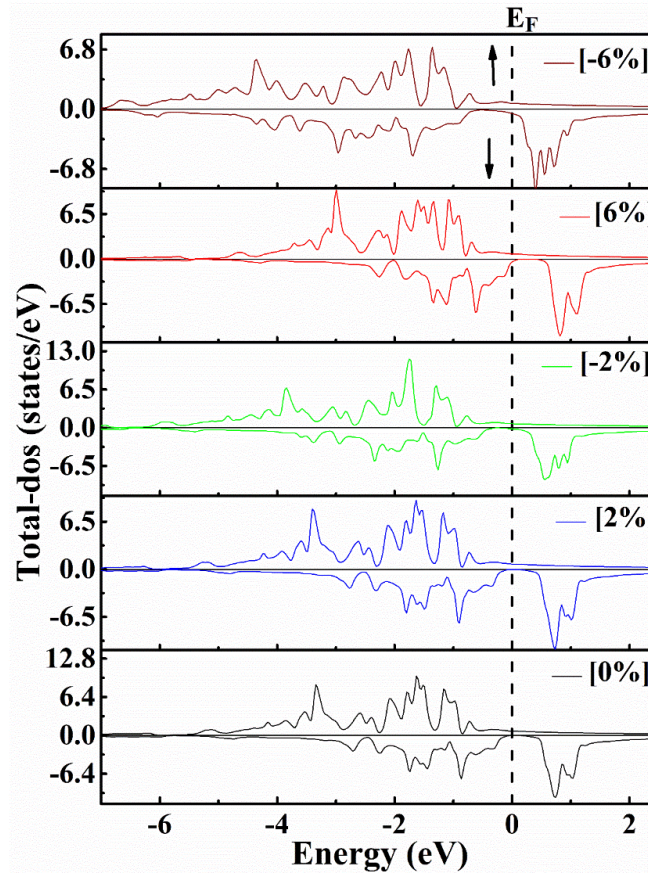


Figure 5. The spin-polarized density of states (DOS) plots of Co₂FeAl alloy under uniform strains. The majority and minority spins are shown by up and down arrows. Fermi level (i.e., $E_F = 0$) is shown by a vertical dashed line. Note that the data are shown only for -6%, -2%, 0%, 2%, and 6%.

Then strains were applied to the system are: -6%, -5%, -4%, -3%, -2%, -1%, up to +6% relative to $a_{\text{(optim.)}}$. Generally, in a layered structure, a significant epitaxial strain is expected from its adjacent layers, resulting in non-uniform strain. That is why we also studied the effects of tetragonal distortions with c axis, which was varied from -6% to +6%, keeping total volume of the cell constant. We have carefully chosen the ranges of distortions to see the trends of the density of states and its effect on half-metallicity as these properties are highly sensitive to the distortions applied. Some reports on band structures are available on unstrained (i.e., cubic) case based on the Co₂FeAl alloy [43, 51, 54-60]. However, some of our calculation results must be addressed in predicting the device compatibility under uniform-strain and tetragonal distortions. Additionally, a systematic comparative study on the phase stability under various magnetic and non-magnetic states is performed. Figure 5 shows the effect of the uniform strains on the DOS. The basic structure of the density of states remains the same which is not astonishing as the basic crystal symmetry is unchanged. Here the main dissimilarity between the DOS's is that the energy gaps shift with respect to the Fermi energy. The gap centers are also slightly changed because of the strains. As we know that for a free electron gas, $E_F \propto V^{-2/3}$, hence a shift in E_F is expected with the unit cell volume. A comparison of all values as obtained from SCF calculations under uniform strains are gathered in Table 3. We have calculated spin polarization (P) as the ratio $[D\uparrow(E_F) - D\downarrow(E_F)] / [D\uparrow(E_F) + D\downarrow(E_F)]$, where $D\uparrow(E_F)$ and $D\downarrow(E_F)$ are the majority (i.e., spin-up) and minority (i.e., spin-dn) density of states at the E_F . The trends of spin polarization, the total magnetic moment per cell and partial moments of Fe and Co, the center position and the gap width are shown in figure 6 (b, a, c) respectively. It can be seen that 100% SP is retained only from 0 to +4% (positive) strain and dropped rapidly from 90% to 16% for negative strains started from -1% to -6%. In figure 6, we have also plotted gap centers with respect to the Fermi energy (E_F) represented by a point and the energy gap (E_{gap}) by error bars.

Table. 3. SCF+ SO results showing spin polarization, the total magnetic moment per cell, partial magnetic moments of Co and Fe, and half-metallic ferromagnetic (HMF) behavior.

Uniform strain %	$\rho\uparrow$ (E_F)	$\rho\downarrow$ (E_F)	P %	M_{Co}	M_{Fe}	M_t ($\mu_B/f.u.$)	HMF
-6%	0.67	0.48	16.52	1.167	2.577	4.76	No
-5%	0.70	0.40	27.27	1.170	2.626	4.83	No
-4%	0.69	0.31	38	1.199	2.664	4.89	No
-3%	0.69	0.23	50	1.207	2.695	4.92	No
-2%	0.69	0.29	40.81	1.220	2.736	4.97	No
-1%	0.73	0.05	87.17	1.215	2.773	4.96	No
0%	0.71	0	100	1.230	2.806	5.0	Yes
+1%	0.72	0	100	1.228	2.815	5.01	Yes
+2%	0.72	0	100	1.235	2.829	5.01	Yes
+3%	0.73	0	100	1.237	2.846	5.01	Yes
+4%	0.74	0	100	1.239	2.865	5.01	Yes
+5%	0.75	0.10	76.47	1.248	2.882	5.05	No
+6%	0.75	0.42	28.20	1.264	2.903	5.10	No

The energy gap is increased from 0.05 eV to 0.13 eV for the strain between 0 to +6%, and decreased from 0.05 eV to .005 eV for the strain between 0 to -6%.

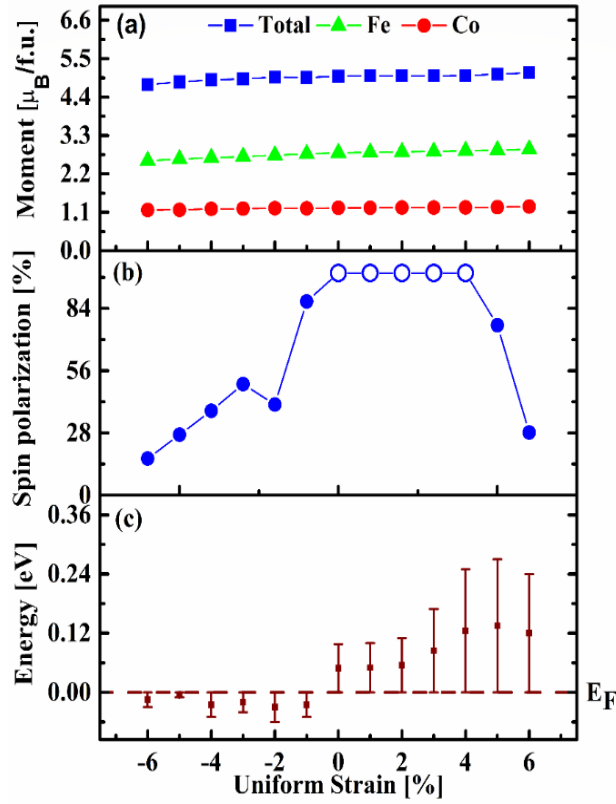


Figure 6. Uniform strain effect on the magnetic moment, spin polarization and band gap for Co_2FeAl are shown in (a), (b), and (c), respectively. 100% spin polarization is shown by a hollow circle, the Fermi energy is represented by a horizontal dashed-line in and the band gap center is shown by a point. The energy gap (E_{gap}) is shown by error bars.

The main reason for the loss of the half-metallicity is due to the shift of the bands with respect to the Fermi energy [35]. When negative strain is applied to the lattice causes it to squeeze. The resulting smaller volume of the unit cell results in broader bands. The dispersions in the electronic states are larger because of the steeper bands. For the positive strain, it is just the opposite. Notice that the above results are with the spin-orbit coupling (SOC). We also noticed, no significant difference in total magnetic moments of the cell with or without SOC during the self-consistent field (SCF) calculations. The gap center and width changes can be explained as follows; exchange coupling will be increased when electrons are more localized and hence, minority bands are shifted at higher with respect to their majority bands. In Figure 6, we can see the variation of the total moments as well as partial moments of the atoms with respect to the strain. From these results, we accomplish that the integer magnetic moment will be the necessary condition to obtain a 100% spin-polarized Heusler alloy.

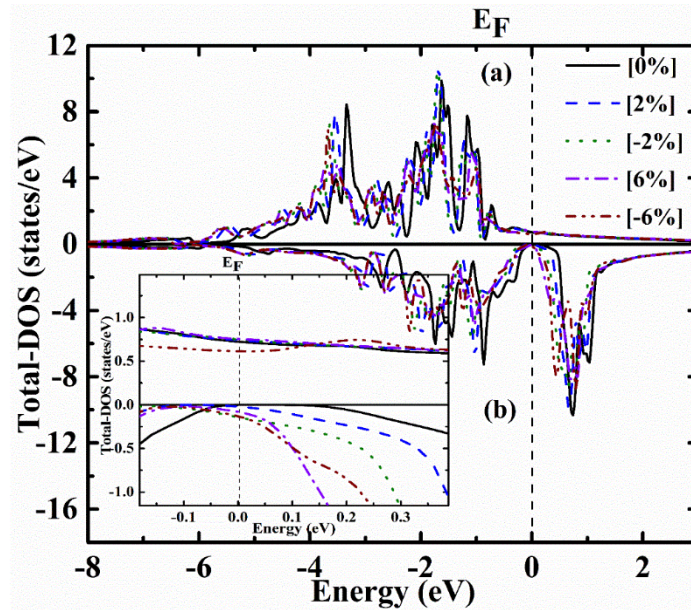


Figure 7. The density of states (DOS) plot of Co_2FeAl alloy under tetragonal distortions are shown of (a) majority and (b) minority spins. Data are shown for -6%, -2%, 0%, 2%, and 6%. Inset represents the magnified version near the E_F .

An unstrained Co_2FeAl Heusler alloy has a total magnetic moment of $5.0 \mu_B$, which is quite consistent with the value predicted by the Slater-Pauling (SP) rule. An integer magnetic moment is retained and hence half-metallicity too, up to when changes in atomic magnetic moments were compensated by each other. Moreover, until the covalent bonding is strong between transition metals, the half-metallicity is preserved, and when it is weakened, resulting in loss of half-metallic behavior. μ_{Co} and μ_{Fe} were decreased for negative strain (see figure 6) so the total magnetic moment of the cell is reduced. On contrary to negative strain, the total magnetic moment slightly increases for the positive strains (see table 3).

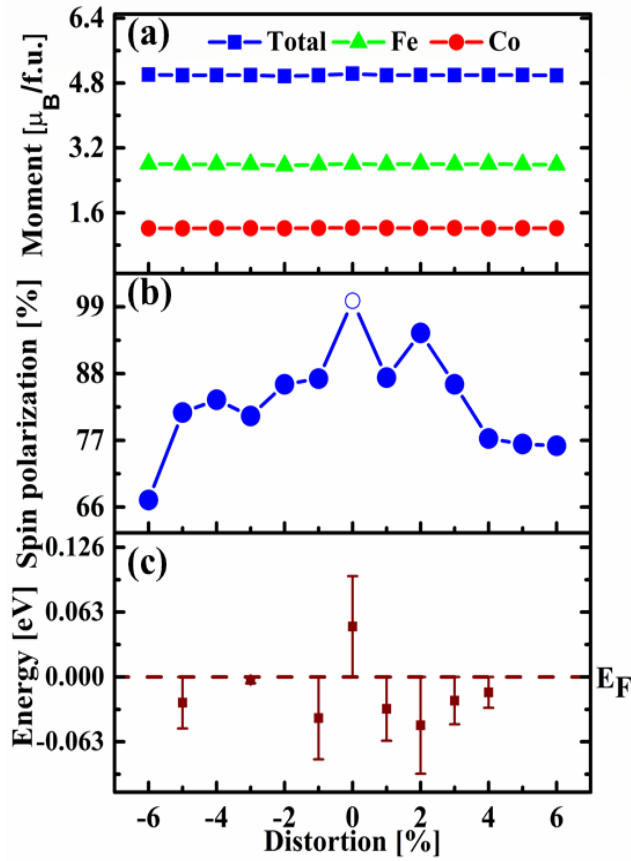


Figure 8. Uniform strain effect on the magnetic moment, spin polarization and band gap for Co_2FeAl are shown in (a), (b), and (c), respectively. 100% spin polarization is shown by a hollow circle, the Fermi energy is represented by a horizontal line in (c) the band gap center is shown by point and E_{gap} is shown by error bars.

The effect of tetragonal distortions upon the total density of states (T-DOS) is presented in figure 7. The general shapes of DOS are not changed. The influence of tetragonal distortion on E_{gap} and spin-polarization (P) are shown in figure 8. We observed that Co_2FeAl alloy is much sensitive under tetragonal distortions and 100% spin polarization is only preserved for zero percent distortion case. The changes in band gaps (E_{gap}) are also shown relative to applied distortions, which is not monotonic. A comparison of all values is given in Table 4. Interestingly, we have noticed that the spin polarization (P) decreases drastically in the case of uniform-strains as compared to the tetragonal distortions. Under uniform-strains, the E_F shifts to the right side of the gap for the negative strains (see figure 5). But for the positive strains, it shifts to the left side of the E_{gap} . On contrary, the E_F only shifts to the right side of the gap under tetragonal distortions. The spin polarization is significantly high under tetragonal distortions as compared with the uniform-strain case (see the table 3&4). The reason might be due to the total magnetic moments were not much deviated from the Slater Pauling rule. Hence we conclude that while half-metallicity (and 100%P) is much sensitive under tetragonal distortions, the spin-polarization values are quite high which is good sign for device application.

Table. 4. SCF+ SO results showing spin polarization, the total magnetic moment per cell, partial magnetic moments of Co and Fe, and half-metallic behavior (HMF).

Distortion %	$\rho\uparrow$ (E_F)	$\rho\downarrow$ (E_F)	P %	M_{Co}	M_{Fe}	M_t ($\mu_B/\text{f.u.}$)	HMF
-6%	0.611	0.12	67.16	1.216	2.810	5.01	No
-5%	0.69	0.07	81.57	1.214	2.791	4.99	No
-4%	0.79	0.07	83.70	1.217	2.794	4.99	No
-3%	0.76	0.08	81.02	1.219	2.793	4.99	No
-2%	0.75	0.14	86.23	1.212	2.762	4.96	No
-1%	0.73	0.05	87.17	1.220	2.791	4.99	No
0%	0.71	0	100.0	1.230	2.806	5.0	Yes
+1%	0.74	0.05	87.34	1.220	2.792	4.99	No
+2%	0.74	0.02	94.71	1.222	2.808	4.99	No
+3%	0.74	0.05	86.23	1.220	2.791	4.99	No
+4%	0.75	0.09	77.30	1.214	2.804	4.99	No
+5%	0.75	0.10	76.47	1.218	2.790	4.99	No
+6%	0.74	0.10	76.10	1.218	2.783	4.99	No

The Loss of 100% spin polarization (P) due to uniform-strain and distortions will affect the device performance, for e.g., thin films prepared by sputtered technique may have stresses of ± 1 GPa because of preparation method alone [61]. Therefore, to get optimal results, vigilant control of deposition techniques are required. Based on our results and discussions following are the criteria of choosing a good spacer layer: (i) it should be of good lattice match with the Heusler alloys (2) a good band matching as well as the long diffusion length are the essential parameter for obtaining expected results in spintronics devices.

4. Conclusion

In summary, we conclude that Co_2FeAl alloy energetically prefers ferromagnetic ground state. Integer magnetic moment is a necessary criterion to obtain a half-metal. Our study suggests a careful choice of substrate or spacer layer is mandatory to achieve expected results in spin-based devices. We have demonstrated that the half-metallicity (HM) of Co_2FeAl is much sensitive to the distortions (uniform/or non-uniform) applied. The reason for the loss of half metallicity (i.e. 100% spin polarization) was due to the shift of the bands with respect to the E_F . In case of tetragonal distortions, the closing of the gap is responsible for the loss of half-metallicity due to weakening of the covalent hybridization between the Co-Fe atoms. We believe that the present study is highly instructive of synthesizing a Heusler based thin films as well as heterostructures.

Acknowledgments

Aquil Ahmad sincerely acknowledges the University Grant Commission (UGC) Delhi, MHRD Delhi, India for providing fellowship for Ph.D. work. A. K. Das acknowledges the financial support of DST, India (project no. EMR/2014/001026). We also acknowledge our departmental computational facility, IIT Kharagpur, India.

References

- [1] de Groot R A, Mueller F M, Engen P G and Buschow K H J 1983 Phys. Rev. Lett. **50** 2024-2027

- [2] Wolf S, Awschalom D, Buhrman R, Daughton J, Von Molnar S, Roukes M, Chtchelkanova A Y and Treger D 2001 Science **294** 1488-1495
- [3] Fang C M, de Wijs G A and de Groot R A, 2002 J. Appl. Phys. **91** 8340
- [4] Picozzi S, Continenza A and Freeman A J 2002 Phys. Rev. B, **66** 094421
- [5] Ishida S, Fujii S, Kashiwagi S and Asano S 1995 J. Phys. Soc. Japan **64** 2152-2157
- [6] Ishida S, Masaki T, Fujii S and Asano S. 1998 Physica B Cond. Matter **245** 1-8
- [7] Ahmad A, Mitra S, Biswas S, Srivastava S K and Das A K 2019 AIP Conf. Proc. **2115** 030508.
- [8] Ahmad A, Das A K and Srivastava S K 2020 Eur. Phys. J. B **DOI:** 10.1140/epjb/e2020-100626-4
- [9] Dahmane F, Mogulkoc Y, Doumi B, Tadjer A, Khenata R., Bin Omran S., Rai D.P., Murtaza G and Varshney D, J. 2016 Magn. Magn. Mater. **407** 167-174
- [10] Datta S. and Das B 1990, Appl. Phys. Lett. **56** 665-667
- [11] Kilian K and Vitoria R 2000 J. Appl. Phys. **87** 7064-7066
- [12] Żuberek R, Chumak O, Nabiałek A, Chojnacki M, Radelytskyi I and Szymczak H 2018 J. Alloys Comp. **748** 1-5
- [13] Sagotra A K Errandonea D and Cazorla C 2017 Nature Commun. **8** 1-7
- [14] Ahmad A, Srivastava S K and Das A K 2019 arXiv:1909.10201
- [15] Mohn P and Supanetz E, 1998 Philosophical Magazine B, **78** 629-636
- [16] de Groot R A, Mueller F M, Van Engen P.G. and Buschow K.H.J., 1984 J. Appl. Phys., **55** 2151-2154.
- [17] Galanakis I, Dederichs P and Papanikolaou N 2002 Phys. Rev. B **66** 174429
- [18] Galanakis I, Dederichs P H and Papanikolaou N 2002 Physical Review B, **66** (2002) 134428
- [19] Galanakis I 2002 J. Phys. Condens. Matter **14** 6329
- [20] Mavropoulos P, Sato K, Zeller R, Dederichs P H, Popescu V and Ebert H 2004 Phys. Rev. B, **69** 054424
- [21] Xie W H, Xu Y Q, Liu B G and Pettifor D G 2003 Phys. Rev. Lett., **91** 037204
- [22] Gupta A and Sun J 1999 J. Magn. Magn. Mater. **200** 24-43
- [23] Ahmad A, Mitra S, Srivastava S K, Das A K 2019 J. Magn. Magn. Mater. **474** 599-604
- [24] de Wijs G.A and de Groot R A 2001 Phys. Rev. B, **64** 020402
- [25] Tanaka C T, Nowak J and Moodera J S, 1999 J. Appl. Phys. **86** 6239-6242

- [26] Soulen R, Byers J, Osofsky M, Nadgorny B, Ambrose T, Cheng S, Broussard P R, Tanaka C, Nowak J and Moodera J, 1998 Science, **282** 85-88
- [27] Bona G, Meier F, Taborelli M, Bucher E and Schmidt P 1985 Solid State commun. **56** 391-394
- [28] Mancoff F, Clemens B. Singley E and Basov D 1999 Phys. Rev. B **60** R12565
- [29] Hanssen K, Mijnders P, Rabou L and Buschow K 1990 Phys. Rev. B **42** 1533
- [30] Caballero J, Reilly A, Hao Y, Bass J, Jr Pratt W, Petroff F and Childress J, 1999 J. Magn. Magn. Mater. **198** 55-57
- [31] Block T, Felser C, Jakob G, Ensling J, Mühling B, Gütlich P and Cava R 2003 J. Solid State Chem., **176** 646-651
- [32] Picozzi S, Continenza A and Freeman A J 2004 Phys. Rev. B, **69** 094423
- [33] Orgassa D, Fujiwara H, Schulthess T and Butler W 1999 Phys. Rev. B **60** 13237
- [34] Carey M, Block T and Gurney B 2004 Appl. Phys. Lett. **85** 4442-4444
- [35] Block T, Carey M, Gurney B and Jepsen O 2004 Phys. Rev. B, **70** 205114
- [36] Wang P, Xia J B, Wei Z, Wen H, Zong Y, Wu H B, 2019 J. Phys. D Appl. Phys. **52** 505003
- [37] Blaha P, Schwarz K, Madsen G, Kvasnicka D and Luitz J 2002 WIEN2K, Vienna University of Technology, ISBN 3-9501031-1-2.
- [38] Fadila B, Ameri M, Bensaid D, Noureddine M, Ameri I, Mesbah S and Al-Douri Y. 2018 J. Magn. Magn. Mater., **448** 208-220
- [39] Rai D, Shankar A, Sandeep J, Singh L, Jamal M, Hashemifar S, Ghimire M and Thapa R 2012 Armenian J. Phys. **5** 105-110
- [40] Ahmad A, Srivastava S K and Das A K 2019 J. Magn. Magn. Mater. **491** 165635
- [41] Perdew J P, Burke K and Ernzerhof M, 1996 Phys. Rev. Lett. **77** 3865
- [42] Birch F 1947 Phys. Rev. **71** 809-824
- [43] Matsushita Y.I., Madjarova G, Dewhurst J K, Shallcross S, Felser C, Sharma S and Gross E K 2017 J. Phys. D Appl. Phys. **50** 095002
- [44] Kokalj A 2003 Comput. Mater. Scie. **28** 155-168
- [45] Aarizou Z, Bahlouli S and Elchikh M 2015 Modern Phys. Lett. B **29** 1550093
- [46] Elmers H J, Wurmehl S, Fecher G H, Jakob G, Felser C and Schönhense G 2004 Appl. Phys. A **79** 557-563

- [47] Ahmad A., Guchhait S, Ahmad H, Srivastava S K and Das A K 2019 AIP Conf. Proc. **2142** 090006
- [48] Errandonea D, Santamaría-Perez D, Vegas A, Nuss J, Jansen M, Rodríguez-Hernandez P and Muñoz A. 2008 Phys. Rev. B **77** 094113
- [49] Saccone F D, Ferrari S, Errandonea D, Grinblat F, Bilovol V and Agouram S 2015 J. Appl. Phys. **118** 075903
- [50] Titov A, Jirásková Y, Zivotsky O, Bursik J, Janickovic D 2018 AIP Advances **8** 047206
- [51] Comtesse D, Geisler B, Entel P, Kratzer P and Szunyogh L 2014 Phys. Rev. B, **89** 094410.
- [52] Elmers H, Wurmehl S, Fecher G, Jakob G, Felser C and Schönhense G 2004 Appl. Phys. A, **79** 557-563
- [53] Galanakis I, Mavropoulos P and Dederichs P H 2006 J. Phys. D Appl. Phys. **39** 765
- [54] Huang T, Cheng X-M, Guan X W and Miao X S 2015 IEEE Transactions on Magnetics, **51** 1-4
- [55] Siakeng L, Mikhailov G M and Rai D P 2018 J. Mater. Chem. C, **6** 10341-10349
- [56] Fadila B, Ameri M, Bensaid D, Noureddine M, Mesbah I and Al-Douri Y, 2018 J. Magn. Magn. Mater. **448** 208-220
- [57] Elmers H J, Wurmehl S, Fecher G H, Jakob G, Felser C and Schönhense G, 2004 J. Magn. Magn. Mater., **272** 758-759.
- [58] Qiao J, Peng S, ZhanY, Yang H, and Zhao W 2018 Phys. Rev. B, **97** 054420.
- [59] Shreder E I, Svyazhin A D, Belozerova K A, 2013 Phys. Metals Metallog. **114** 904-909
- [60] Shreder E I, Lukoyanov A V, Marchenkov V V, 2016 Phys. Solid State **58** 164-169
- [61] Vink T J, Somers M A J, Daams J L C and Dirks A G 1991 J. Appl. Phys. **70** 4301-4308